Dynamical Behavior of Initially Stressed Generalized Magneto-thermoelastic Models under the Effect of Nonlocality and Two Temperature Parameter

Sonia Bajaj* [1,2], A. K. Shrivastav [1]

[1]Department of Mathematics, MMEC, Maharishi Markandeshwa (Deemed to be University) Mullana,
Ambala, Haryana, India

[2]Department of Mathematics, Chandigarh University, Mohali, India
bajajsonia1501@gmail.com*, aakkaasshhkumar8888@gmail.com,

Abstract. The effect of nonlocal and two-temperature parameter on an initially stressed generalized magneto-thermoelastic solid with gravity has been discussed. The problem is studied using Green-Naghdi (GN II), Lord-Shulman (L-S), and the three phase lag (TPL) models. The governing equations are solved by the normal mode method, and analytic solutions are obtained for representations of the displacement, force stress tensors, and temperatures. The effects on physical fields are observed when suitable boundary conditions are applied. MATLAB software has been used for the calculation and execution of numerical computations. Comparative graphical analysis is shown for three different theories in the presence and absence of two temperature parameter. The numerical findings for the quantities of fields that are physical domains are visually displayed in the presence and absence of the nonlocal parameter.
In summary, two temperature and nonlocal thermoelasticity significantly impact the physical variables.
Keywords: Gravity, initial stress, magnetic field, thermoelasticity, three-phase lag model, two temperature theory.

1. Introduction

The field of generalized thermoelasticity has evolved to address the limitation of infinite thermal signal propagation speeds as existing in classical coupled dynamical thermoelasticity [1]. This area encompasses a broad spectrum of advancements beyond the traditional theory of thermoelasticity. Among the earliest and most prominent models in this domain are those introduced by Lord-Shulman [2] ; Green-Lindsay [3]. In L-S framework, the Maxwell-Cattaneo law replaced the Classical Fourier law (CFL) by incorporating a single relaxation time parameter. Conversely, the The g-L model introduced two relaxation parameters, inside stress tensor and entropy in the constitutive relations, offering a more comprehensive description. Subsequent studies have further refined these theories; for instance, Abbas and Zenkour [4] explored the electromagneto-thermoelastic behavior of functionally graded cylinder with infinite length in the framework of the L-S model. Other

© The Author(s) 2026
S. Kumar et al. (eds.), *Proceedings of the 2nd International Conference on Advanced Materials & Devices for Futuristic Applications-2024 (IC-AMDFA 2024)*, Atlantis Highlights in Materials Science and Technology 5,
https://doi.org/10.2991/978-94-6239-695-1_10

significant contributions include research by Chandrasekharaiah [5], who reviewed various generalized thermoelasticity theories, and Tzou [6], who proposed dual-phase-lag (DPL) model to account for microscopic and macroscopic heat conduction phenomena. These studies have significantly expanded the understanding and applicability of generalized thermoelasticity in complex physical scenarios.

In subsequent years, Green-Naghdi [7-9] introduced three additional models of thermoelasticity, now commonly referred as the GN I, II, III. The linear representation of GN I aligns with the classical thermoelastic theory. GN II is distinctive in that it assumes the internal entropy production rate to be identically zero, which implies the absence of thermal energy dissipation (TWED). GN II is particularly noteworthy for admitting undamped thermoelastic waves in materials, making it widely recognized as the theory of TWED. GN III, on the other hand, is a more generalized framework that encompasses the first two models as special cases and permits energy dissipation. Abbas and Zenkour [10] conducted an in-depth analysis of the magnetic field's impact in a fiber-reinforced half-space which is anisotropic by using GN theory. Other notable works in this area include those by Quintanilla [11], who studied uniqueness and stability in GN theories, and Dhaliwal and Singh [12], who explored wave propagation and thermoelastic interactions under generalized models. These studies have greatly advanced the theoretical and practical understanding of thermoelasticity in diverse materials and applications.

Choudhuri [13] introduced an innovative model in the realm of thermoelasticity, which is referred as TPL model. This model modifies the CFL by incorporating with an estimated value as described by the equation:

$$q\big(P,\tau_q + t\big) = -k^*\tau_v \nabla v(P,\tau_v + t) - k\nabla T(P,\tau_T + t),$$

where q represents the heat flux vector, T represents the temperature, and v denotes displacement due to temperature change, satisfying the relation $T = \dot{v}$. The equation highlights that the heat flux vector at a given point and time $\big(\tau_q + t\big)$ depends on both the temperature gradient at $(\tau_T + t)$ and the gradient of the thermal displacement at $(\tau_v + t)$. The time delays, τ_q, τ_T, and τ_v, arise due to microstructural interactions like phonon scattering and electron-phonon interactions, interpreted as relaxation times induced by fast transient thermal inertia impacts.

Choudhuri's objective was to construct a mathematical framework which incorporates different phase lags i.e. lag in heat flux, thermal displacement gradient, and temperature gradient. By employing various Taylor approximations, this model can recover earlier theories, including GN theories. The TPL model also extends DPL model introduced by Tzou [6], making it a versatile approach to addressing complex thermal phenomena. Its applications span areas such as nuclear boiling, microstructural heat transport, and exothermic catalytic reactions.

Several researchers have contributed to advancing the TPL theory. Quintanilla and Racke [14] analyzed the solution's stability of TPL model. Kanoria and Mallik [15] applied it to solve thermoelasticity problems, while El-Karamany and Ezzat [16] explored its implications in advanced materials. Additionally, Liao, Zhang, and Wu, along with Ezzat, El-Karamany, and Fayik [17], investigated its applications in

dynamic thermoelastic problems. These studies underscore the robustness and adaptability of the TPL model across diverse scientific and engineering disciplines.

Initial stresses within solids play a crucial role in influencing the response of materials to mechanical load while transitioning from an initially stressed structure. These stresses have significant approaches in fields such as geophysics, the analysis of engineering frameworks, and the study of biological skin tissues. Pre-existing stresses are intrinsic to materials and arise due to processes like manufacturing, thermal expansion, or biological growth, existing even in absence of external loads.

Montanaro [18] developed a theoretical framework for isotropic thermoelasticity that incorporates hydrostatic initial stress, providing a foundational approach for analyzing such conditions. Subsequent studies have extended this theory to explore various dynamic and wave propagation phenomena. Othman and Song [19] and Singh [20] applied Montanaro's model to examine the behavior of plane waves within the generalized thermoelasticity, thereby enhancing the understanding of wave mechanics in stressed materials.

Other researchers have also made significant contributions to this field. ZH Qian [21], studied the effect of Pre-existing stress on functionally graded materials, while Ibrahim A. Abbas [22] also analyzes the effect of earlier stress and relaxation time on physical parameters in a thermoelastic half-space along with voids under a thermal source and are solved by using the finite element method. Iqbal Kaur [23] observed the effects of time-harmonic on displacement and stress components. It also observed the variations of temperature in a transversely isotropic magneto-thermoelastic solid with initial stress under mechanical and thermal loads.

Magneto-thermoelasticity explores the interplay between magnetic fields and the thermoelastic deformations of solid materials. This field has garnered significant attention because of its relevance in nuclear devices that have primary magnetic fields. Such studies also hold importance in biomedical engineering and geomagnetic research by analyzing the coupled effects of magnetic, thermal, and strain fields. Early developments in this area, such as those by Paria [24], laid the foundation for subsequent advancements.

Recent works have focused on incorporating thermal relaxation times and advanced modeling techniques. Sadeghi [25] focused on developing and solving the generalized magneto-thermoelastic response generated from the layer, incorporating two generalised theories., while Tiwari [26] examined the impact of phase lags on magneto-thermoelastic behavior in a solid in context to a moving source of heat, and Yadav [27] analyzed wave reflection in a magnetized rotation, triclinic half-space under a temperature field, identified three quasi-waves and examined the coupled waves reflection on a insulated thermal surface.

Additional contributions include abouelregal [28], who analyzed the interactions in a viscoelastic rotating rod under magnetic feild subject to the heat source in movement. and singh [29], analysed and conducted to explore the influence of gravity, pre-existing stress, and magnetic fields on the propagation of Rayleigh waves within a uniform orthotropic magneto-thermoelastic medium, employing the TPL model in conjunction with a dual-temperature framework.

According to Eringen's nonlocal elasticity theory [30-32], in nonlocal elasticity, the stress tensor at a point in a nanomaterial depends not only on the strain at that point but also on contributions from the entire material. For isotropic, elastic, and homogeneous materials without body forces, the stress-strain relationship accounts for these nonlocal interactions. The fundamental equation of nonlocal elasticity for isotropic, elastic, and homogeneous materials, in the absence of body forces, is expressed as a relationship where the stress depends on the strain at that point and contributions from the surrounding material. The nonlocal elasticity theory, as formulated by Eringen, expresses the stress tensor $\boldsymbol{\tau}(\mathbf{x})$ at a point $\mathbf{x}$ as a function of the weighted average of stresses $\boldsymbol{\sigma}(\mathbf{x})$ over the entire domain. The integral form is given by:

$$\boldsymbol{\tau}(\mathbf{x}) = \int_V \alpha' \boldsymbol{\sigma}(\mathbf{x}')(|\mathbf{x} - \mathbf{x}'|, \xi) dV(\mathbf{x}')$$

where the kernel function α' describing the nonlocal influence and ξ is the nonlocal parameter.

The strain tensor ($\boldsymbol{\varepsilon}$) is expressed in terms of displacement vector($\mathbf{u}$)as:

$$\boldsymbol{\varepsilon} = \frac{(\nabla \mathbf{u}^{\mathsf{T}} + \nabla \mathbf{u})}{2}$$

Constitutive relation :

$$2\mu\boldsymbol{\varepsilon} + \lambda(\nabla \cdot \mathbf{u})\mathbf{I} - \gamma\theta\mathbf{I} = \boldsymbol{\sigma}$$

Lamé constants (μ & λ), the thermal modulus (γ), temperature change (θ), are related as expressed in above relation where ($\mathbf{I}$) is the identity tensor.

Nonlocal stress tensor $\boldsymbol{\tau}(\mathbf{x})$ can also be shown in a simplified differential form as:

$$(1 - \xi^2\nabla^2)\boldsymbol{\tau}(\mathbf{x}) = \boldsymbol{\sigma}(\mathbf{x})$$

This equation accounts for the size effect on the mechanical behavior of nanostructures.

Equation of motion:

$$\mathbf{F} + \nabla \cdot \boldsymbol{\tau} = \rho\ddot{\mathbf{u}}$$

where $\mathbf{F}$ vector denotes the external body force, ρ is the mass density, and $\ddot{\mathbf{u}}$ represents the material acceleration.

Using the nonlocal stress relationship above equation can be expressed as:

$$\nabla \cdot \boldsymbol{\sigma} + (1 - \xi^2\nabla^2)\mathbf{F} = \rho(1 - \xi^2\nabla^2)\ddot{\mathbf{u}}$$

or

$$\rho(1 - \xi^2\nabla^2)\ddot{\mathbf{u}} = \mu\nabla^2\mathbf{u} + (\mu + \lambda)\nabla(\nabla \cdot \mathbf{u}) - \gamma\nabla\theta + (\mathbf{F} - \xi^2\nabla^2\mathbf{F})$$

Wang and Dhaliwal [33] formulated the energy and work equations within the context of nonlocal generalized thermoelasticity and established the existence and uniqueness of solutions for boundary and initial value problems. Zenkour and Abouelregal [34] proposed a novel non-local thermoelasticity model with phase lags for beam theory, Considering a periodically fluctuating heat source and integrating varying thermal conductivity. Many renowned researchers [35-40] contributed in this field.

The current study focuses on analyzing displacement, stress, temperature and potential distributions in an isotropic, homogeneous, initially stressed elastic solid

under mechanical and thermal loads, using the generalized electro-magneto-thermoelastic theory within the TPL model. The problem is expressed in a dimensionless form and solved analytically using normal mode analysis. Numerical results for copper parameters are displayed graphically to demonstrate the impacts of initial stress and magnetic fields.

2. Mathematical Framework

The present study examines a thermoelastic, isotropic, homogeneous, linear half-space that is thermally and electrically conductive, influenced by gravity, with the z-axis directed vertically inward. The surface of the half-space ($z = 0$) is free from traction and experiences mechanical and thermal loading. All functions remain finite as $z \to \infty$, and the medium is maintained at a uniform temperature T_0. A primary magnetic field, $\mathbf{H}_0 = (0, H, 0)$, is applied along the positive y-axis, inducing both a magnetic field **h** and an electric field **E** within the material.

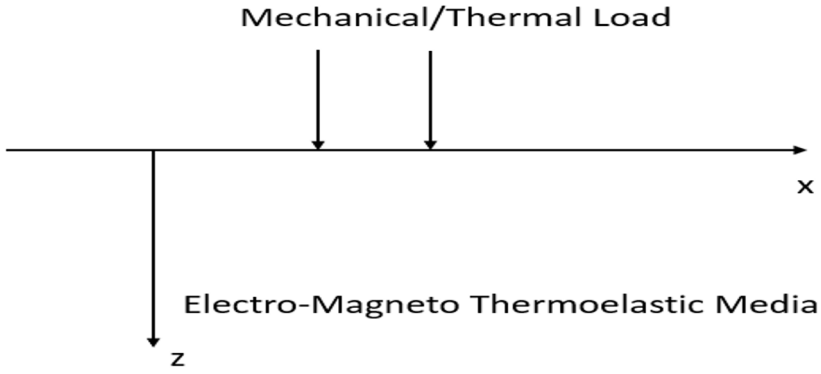

Fig. 1. Geometry of Problem

Constitutive relations

$$(1 - e^2\nabla^2)\sigma_{ij} = \mu\left(u_{j,i} + u_{i,j}\right) - pw_{ij} + \left(\lambda u_{r,r} - \beta_1 T - p\right)\delta_{ij}, \tag{1}$$

Maxwell's equations governing the electromagnetic fields in the material are given by:

$$\nabla \times \mathcal{H} = \mathcal{J} + \epsilon_0\dot{\mathcal{E}}, \quad \nabla \times \mathcal{E} = -\mu_0\dot{\mathcal{H}}, \quad \mathcal{E} = -\mu_0\left(\dot{\mathcal{U}} \times \mathcal{H}\right), \quad \nabla \cdot \mathcal{H} = 0.$$

From these equations, the following are derived:

$$\mathcal{E} = \mu_0 H_0\left(\dot{\mathcal{U}}_z, 0, -\dot{\mathcal{U}}_x\right), \quad \mathcal{H} = (0, -H_0\varepsilon_x, 0),$$

$$\mathcal{J} = \left(-\mathcal{H}_{,z} - \epsilon_0\mu_0 H_0\ddot{\mathcal{U}}_z, 0, \mathcal{H}_{,x} + \epsilon_0\mu_0 H_0\ddot{\mathcal{U}}_x\right).$$

The Lorentz force is expressed as:

$$\mathcal{F}_i = \mu_0(\mathcal{J} \times \mathcal{H})_i.$$

From the relations, the force vector components are:

$$\mathcal{F} = \left(\mathcal{F}_x, \mathcal{F}_y, \mathcal{F}_z\right) = \left(\mu_0 H_0^2\varepsilon_{,x} - \epsilon_0\mu_0^2 H_0^2\ddot{\mathcal{U}}_x, 0, \mu_0 H_0^2\varepsilon_{,z} - \epsilon_0\mu_0^2 H_0^2\ddot{\mathcal{U}}_z\right) \tag{2}$$

Equations of motion

$$\left(\mu - \frac{p}{2}\right)\nabla^2 \vec{u} + \left(\lambda + \frac{p}{2} + \mu + \mu_0 H_0^2\right)\nabla(\nabla.\vec{u}) + \vec{F} - \beta_1 \nabla T$$

$$= \rho_0(1 - e^2\nabla^2)\left(1 + \frac{\epsilon_0 \mu_0^2 H_0^2}{\rho_0}\right)\frac{\partial^2 \vec{u}}{\partial t^2}, \quad (3)$$

Equation of thermal conductivity [13]

$$K^*\nabla^2(\varphi) + \tau_v^*\nabla^2(\varphi_{,t}) + K\tau_T\nabla^2(\varphi_{,tt}) = \left(1 + \tau_q\frac{\partial}{\partial t} + \frac{\tau_q^2}{2}\frac{\partial^2}{\partial t^2}\right)\left(\rho C_E T_{,tt} + T_0\gamma_1 u_{i,itt}\right) \quad (4)$$

The relationship between conductive temperature and thermodynamic temperature highlights how heat conduction affects temperature distribution in a medium. Conductive temperature refers to the spatial variation of temperature due to heat transfer, while thermodynamic temperature is an absolute measure of thermal energy. These two are connected through the heat conduction equation, which considers material properties, thermal gradients, and boundary conditions. Thermodynamic temperature often serves as the reference state for analyzing conductive heat flow.

$$\varphi = a\nabla^2(\varphi) + T \quad (5)$$

where σ_{ij} represents components of stress. a represents parameter for two temperature. T, and T_0, are the medium temperature at normal state, and absolute temperature whereas K represents thermal conductivity. C_* reflects constant strain of specific heat. T and θ thermodynamic and conductive temperatures. (τ_T, τ) are temperature gradient and heat flux phase lags respectively, (μ, λ) are Lame's constants. ρ_0 represents the density of the medium. u_i are displacement vector components and , t represents time derivative and δ_{ij} is Kronecker delta function.$\tau_v^* = K + \tau_v * K^*$ and K^* is aditional material constant.

Three phase lag model: $K^* > 0,\ 0 < \tau_v < \tau_T < \tau_q$.

Green Naghdhi's II: $\tau_q = 0,\ \tau_T = 0,\ \tau_v = 0,\ \tau_v^* = K^*\tau_v$ and K=0.

LS theory: $\tau_q^2 = 0,\ \tau_T = 0,\ K^* = 0,\ \tau_v = 0,\ \tau_v^* = K$.

3. Problem Formulation

Considering a two-dimensional space ($z \geq 0$) for a homogeneous isotropic, nonlocal thermoelasticity with initial stress, gravity, and two temperature. Origin is taken randomly on a flat surface considering the positive direction of the Z-axis as vertical downwards in the surface of half-space z=0 as shown in figure of geometry of problem. We take directional components of displacement $\vec{u}$ in rectangular Cartesian coordinate system as

$$u = u_x, v = v_y = 0, w = u_z. \quad (6)$$

The following equations are obtained by combining equations (3), (4), and (6) with gravitational effect.

$$\left(\lambda + \mu + \frac{p}{2} + \mu_0 H_0^2\right)\frac{\partial}{\partial x}\left(\frac{\partial u}{\partial x} + \frac{\partial w}{\partial z}\right) + \left(\mu - \frac{p}{2}\right)\nabla^2 u$$
$$-\beta_1\frac{\partial T}{\partial x} + g(1 - e^2\nabla^2)\frac{\partial w}{\partial x} = \rho_0(1 - e^2\nabla^2)\left(1 + \frac{\epsilon_0\mu_0^2 H_0^2}{\rho_0}\right)\frac{\partial^2 u}{\partial t^2}, \quad (7)$$

$$\left(\lambda+\mu+\frac{p}{2}+\mu_0H_0^2\right)\frac{\partial}{\partial z}\left(\frac{\partial u}{\partial x}+\frac{\partial w}{\partial z}\right)+\left(\mu-\frac{p}{2}\right)\nabla^2 w$$
$$-\beta_1\frac{\partial T}{\partial z}-g(1-e^2\nabla^2)\frac{\partial u}{\partial x}=\rho_0(1-e^2\nabla^2)\left(1+\frac{\epsilon_0\mu_0^2H_0^2}{\rho_0}\right)\frac{\partial^2 w}{\partial t^2}, \tag{8}$$

Acquaints dimensionless quantities as follow [41]

$$\frac{w^*}{c_1}(z,x,w,u)=(z',x',w',u'),\theta'=\frac{\beta_1}{\rho c_0^2}(T-T_0)$$
$$\left(\sigma_{ij'},p'\right)=\frac{\left(\sigma_{ij'}p\right)}{\beta_1T_0},w^*\left(t,\tau_v,\tau_T,\tau_q\right)=\left(t',\tau_{v'},\tau_{T'},\tau_{q'}\right), \tag{9}$$
$$\varphi'=\frac{\beta_1}{\rho c_0^2}\varphi,g'=\frac{g}{c_1w^*},w^*=\frac{\rho C_*c_1^2}{K},c_1^2=\frac{\lambda+2\mu}{\rho}$$

Displacement components can be expressed by using Helmholtz decomposition

$$w=-\frac{\partial(\psi)}{\partial x}+\frac{\partial(q)}{\partial z},\ u=\frac{\partial(\psi)}{\partial z}+\frac{\partial(q)}{\partial x}\text{,,} \tag{10}$$

where $\{q,\ \psi\}$(x,z,t) are scalar potentials. Rewriting equations (4), (7), (8) in dimensionless notations using (9) and applying Helmholtz decomposition (10) ,we get

$$\left[(1+R_H)\nabla^2-(1-e^2\nabla^2)\beta^2\frac{\partial^2}{\partial t^2}\right]q-\theta-g(1-e^2\nabla^2)\frac{\partial\psi}{\partial x}=0, \tag{11}$$

$$\left[(1+R_H)\nabla^2-(1-e^2\nabla^2)\beta^2\frac{\partial^2}{\partial t^2}\right]\psi+g(1-e^2\nabla^2)\frac{\partial q}{\partial x}=0, \tag{12}$$

$$\left[C_k+C_v\frac{\partial}{\partial t}+\tau_T\frac{\partial^2}{\partial t^2}\right]\nabla^2\varphi=\left(1+\tau_q\frac{\partial}{\partial t}+\frac{\tau_q^2}{2}\frac{\partial^2}{\partial t^2}\right)\left[\ddot{\theta}+\epsilon_1\nabla^2\ddot{q}\right] \tag{13}$$

$$\theta=\varphi-n_1\nabla^2\varphi. \tag{14}$$

Where

$$R_H=\frac{V_A^2}{c_0^2},\quad \beta^2=1+\frac{V_A^2}{C^2},\quad V_A^2=\frac{\mu_0H_0^2}{\rho},$$
$$C^2=\frac{1}{\varepsilon_0\mu_0},\quad C_k=\frac{k^*}{\rho C_ec_0^2},\quad C_v=1+C_k\tau_v,\epsilon_1=\frac{\beta_1^2T_0}{\rho^2C_ec_0^2},n_1=\frac{aw^{*2}}{c_0^2}$$

Putting the value of T from (14) into (11) and (13) equations

$$\left[(1+R_H)\nabla^2-(1-e^2\nabla^2)\beta^2\frac{\partial^2}{\partial t^2}\right]q-(1-n_1\nabla^2)\varphi-g(1-e^2\nabla^2)\frac{\partial\psi}{\partial x}=0, \tag{15}$$

$$\left[C_k+C_v\frac{\partial}{\partial t}+\tau_T\frac{\partial^2}{\partial t^2}\right]\nabla^2\varphi=\left(1+\tau_q\frac{\partial}{\partial t}+\frac{\tau_q^2}{2}\frac{\partial^2}{\partial t^2}\right)[(1-n_1\nabla^2)\ddot{\varphi}+\epsilon_1\nabla^2\ddot{q}] \tag{16}$$

4. Solution By Normal Mode Approach

The solution of considered physical variables (following [41]) using the normal mode approach is

$$\{q,\psi,\varphi\}(x,z,t)=\left\{\tilde{q},\tilde{\psi},\tilde{\varphi}\right\}(z)e^{(imx+wt)}, \tag{17}$$

where all the functions with sign in above equation represent the function amplitude, w is angular spin, and m represents serial number of wave along the X-axis. Replacing the solutions (17) into equations (12), (15), and (16) we get the following three equations to solve simultaneously.

$$(O_1D^2-O_2)\tilde{\psi}-(O_3D^2-O_4)\tilde{q}=0, \tag{18}$$

$$(O_1D^2 - O_2)\tilde{q} + (O_3D^2 - O_4)\tilde{\psi} + (O_5D^2 - O_6)\tilde{\varphi} = 0, \tag{19}$$

$$(O_7D^2 - O_8)\tilde{\varphi} - (O_9D^2 - O_{10})\tilde{q} = 0. \tag{20}$$

Where $D = \frac{d}{dz}$,

$O_1 = 1 + R_H + \beta^2 w^2 e^2, O_2 = (1 + R_H)m^2 + \beta^2 w^2(1 + e^2 m^2), O_3 = \iota g m e^2,$

$O_4 = g\iota m(1 + m^2 e^2), O_5 = n_1, O_6 = 1 + m^2 n_1, O' = C_k + C_v w + \tau_T w^2,$

$O'' = 1 + w\tau_q + \frac{\tau_q^2}{2} w^2 O_7 = O' + n_1 w^2 O'', O_8 = O'^{m^2} + O''(1 + n_1 m^2)w^2,$

$O_9 = O''\epsilon_1 w^2, O_{10} = -O''\epsilon_1 m^2 w^2.$

Solving homogeneous equations (18)-(20) for non trivial solutions by taking derivative of coefficients of $(\tilde{\psi}, \tilde{q}, \tilde{\varphi})$ equal to zero, the following six order differential equation is obtained which further is solved to get $k_i^2 (i = 1,2,3,4)$ as eigenvalues:

$$(D^6 + L_1 D^4 + L_2 D^2 + L_3)(\tilde{\psi}, \tilde{q}, \tilde{\varphi}) = 0 \tag{21}$$

where

$V_1 = O_3^2 O_7 + O_1^2 O_7 + O_1 O_5 O_9, V_4 = O_4^2 O_8 + O_8 O_2^2 + O_2 O_6 O_{10},$

$V_2 = 2O_3 O_4 O_7 + O_3^2 O_8 + 2O_1 O_2 O_7 + O_1^2 O_8 + O_1 O_5 O_{10} + O_1 O_6 O_9 + O_5 O_2 O_9$

$V_3 = O_4^2 O_7 + 2O_3 O_4 O_8 + O_2^2 O_7 + 2O_1 O_2 O_8 + O_1 O_6 O_{10} + O_2 O_5 O_{10} + O_2 O_6 O_9$

$L_1 = \frac{V_2}{V_1}, L_3 = \frac{V_4}{V_1}, L_2 = \frac{V_3}{V_1}.$

The solutions of the differential equation (17), as $z \to \infty$

$$(\tilde{\psi}_{(r=1)}, \tilde{q}_{(r=0)}, \tilde{\varphi}_{(r=2)})(z) = \sum_{n=1}^{3} E_{r_n} M_n e^{-k_n z}. \tag{22}$$

Where M_n is function of w and m, n varies from 1 to 3

$$E_{1n} = \frac{O_3 k_n^2 - O_4}{O_1 k_n^2 - O_2}, E_{2n} = \frac{O_9 k_n^2 - O_{10}}{O_7 k_n^2 - O_8}, E_{0n} = 1.$$

Stresses can be represented using (1), (7) and (9) as

$$\sigma_{zz} = P_1 \frac{\partial^2 q}{\partial z^2} - (P_1 - P_2)\frac{\partial^2 \psi}{\partial z \partial x} + P_2 \frac{\partial^2 q}{\partial x^2} - P_1(1 - n_1 \nabla^2)\varphi - p, \tag{23}$$

$$\sigma_{zx} = (P_3 + P_4)\frac{\partial^2 q}{\partial z \partial x} - P_3 \frac{\partial^2 \psi}{\partial x^2} + P_4 \frac{\partial^2 \psi}{\partial z^2}, \tag{24}$$

where

$$P_1 = \frac{\rho c_0^2}{\beta_1 T_0}, P_2 = \frac{\lambda}{\beta_1 T_0}, P_3 = \left(\frac{\mu}{\beta_1 T_0} + \frac{p}{2}\right), P_4 = \left(\frac{\mu}{\beta_1 T_0} - \frac{p}{2}\right).$$

Applying normal mode analysis to stress and displacement components equations (23), (24) and (10), yield as

$$\tilde{\sigma}_{zz} = (P_1 D^2 - m^2 P_2)\tilde{q} + \iota m(P_2 - P_1)D\tilde{\psi} + P_1(n_1(D^2 - m^2) - 1)\tilde{\varphi} - p, \tag{25}$$

$$\tilde{\sigma}_{zx} = \iota m(P_3 + P_4)D\tilde{q} + (P_3 m^2 + P_4 D^2)\tilde{\psi}, \tag{26}$$

$$\tilde{u} = \iota m\tilde{q} + D\tilde{\psi}, \ \tilde{w} = D\tilde{q} - \iota m\tilde{\psi}. \tag{27}$$

Using solution (22) equations (25)-(27) and (14) can be described as

$$\left(\tilde{\sigma}_{zz_{(r=3)}}, \tilde{\sigma}_{zx_{(r=4)}}, \tilde{u}_{(r=5)}, \tilde{w}_{(r=6)}, \tilde{\theta}_{(r=7)}\right) = \sum_{n=1}^{3} E_{rn} M_n(m, w) e^{-k_n z} - s_r p. \tag{28}$$

where $s_r = 1$ for $r = 3$ and 0 otherwise

$$E_{3n} = P_1 k_n^2 - P_2 m^2 + (P_1 - P_2)\iota k_n m E_{1n} + P_1(-1 + n_1(k_n^2 - m^2)E_{2n}),$$
$$E_{4n} = -im(P_3 + P_4)k_n + P_3 m^2 E_{1n} + k_n^2 P_4 E_{1n},$$
$$E_{5n} = im - k_n E_{1n}, \qquad E_{6n} = -k_n - imE_{1n}$$
$$E_{7n} = E_{2n}\left(1 - n_1(k_n^2 - m^2)\right).$$

5. Mechanical And Thermal Boundary Conditions

The boundary condition at z=0 are applied to find M_1, M_2, M_3.

$$\sigma_{zz} = -F_1(x,t) = f_1 e^{(imx+wt)} + p, \tag{29}$$

$$\sigma_{zx} = 0, \tag{30}$$

$$\frac{\partial \varphi}{\partial x} = 0. \tag{31}$$

Equations (28) for r = 3, 4, (22) for r=2 transform to a non-homogeneous set of equations by above mentioned the boundary conditions.

$$\begin{bmatrix} E_{31} & E_{32} & E_{33} \\ E_{41} & E_{42} & E_{43} \\ k_1 E_{21} & k_2 E_{22} & k_3 E_{23} \end{bmatrix} \begin{bmatrix} M_1 \\ M_2 \\ M_3 \end{bmatrix} = \begin{bmatrix} -f_1 \\ 0 \\ 0 \end{bmatrix} \tag{32}$$

The solution of the above set of equations is generated using Cramer's rule.

$$M_n = \frac{\Delta_n}{\Delta};\ n = 1,2,3. \tag{33}$$

$$\Delta = E_{31}[k_3 E_{42} E_{23} - k_2 E_{43} E_{22}] - E_{32}[k_3 E_{41} E_{23} - k_1 E_{21} E_{43}] + E_{33}[k_2 E_{41} E_{22} - k_1 E_{42} E_{21}],$$

Where

$$\Delta_1 = -f_1[k_3 E_{42} E_{23} - k_2 E_{22} E_{43}],$$
$$\Delta_2 = f_1[k_3 E_{41} E_{23} - k_1 E_{21} E_{43}], \Delta_3 = -f_1[k_2 E_{41} E_{22} - k_1 E_{21} E_{42}].$$

Substituting values of M_n into equations (22) and (28)

$$\left(\tilde{\psi}_{(r=1)}, \tilde{q}_{(r=0)}, \tilde{\varphi}_{(r=2)}, \tilde{\sigma}_{z_{z(r=3)}}, \tilde{\sigma}_{z_{x(r=4)}}, \tilde{u}_{(r=5)}, \tilde{w}_{(r=6)}, \tilde{\theta}_{(r=7)}\right)(z) = \frac{1}{\Delta}\sum_{n=1}^{3} \Delta_n E_{r_n} e^{-k_n z}. \tag{34}$$

6. Numerical Discussions

This study conducts a numerical simulation of a initially stressed magneto-thermoelastic solid with gravity while considering the effects of two temperature and nonlocal parameters. The simulations are validated by comparing them with analytical results, ensuring their accuracy. Copper is used as a reference material to illustrate the findings and provide practical insights into the behavior of such solids under these conditions. The relevant material constants (following[42]), expressed in SI units, are as follows:

$$\lambda = 1.76 \times 10^{10} \frac{\mathrm{N}}{\mathrm{m}^2}, \quad \mu = 1.78 \times 10^{10} \frac{\mathrm{N}}{\mathrm{m}^2}, \rho = 1740 \frac{\mathrm{kg}}{\mathrm{m}^3},$$
$$f_0 = 0.05, C_E = 383.3 \frac{\mathrm{J}}{\mathrm{kg}}.\mathrm{K}, T_0 = 293\ \mathrm{K}, \tau_\theta = 7 \times 10^{-5}\ \mathrm{s},$$
$$\tau_q = 9 \times 10^{-5}\ \mathrm{s}, \quad \tau_v = 5 \times 10^{-5}\ \mathrm{s}, \alpha_t = 1.78 \times 10^{-4}\ \mathrm{K}^{-1},$$

$$K^* = 386.3\frac{\mathrm{W}}{\mathrm{m}}.\mathrm{K}, \quad K = 386.6\frac{\mathrm{W}}{\mathrm{m}}.\mathrm{K}, m = m_0 + i\xi, \quad \xi = -0.5,$$

The numerical data mentioned earlier was used to analyze the distribution of the real part of the displacement components u and w, as well as the stresses σ_{zz}, and σ_{xz}, the thermodynamic temperature θ, and the conductive temperature φ for the given problem. For simplicity, all the variables were considered in non-dimensional form. The results of this analysis are presented in figures 2–16.

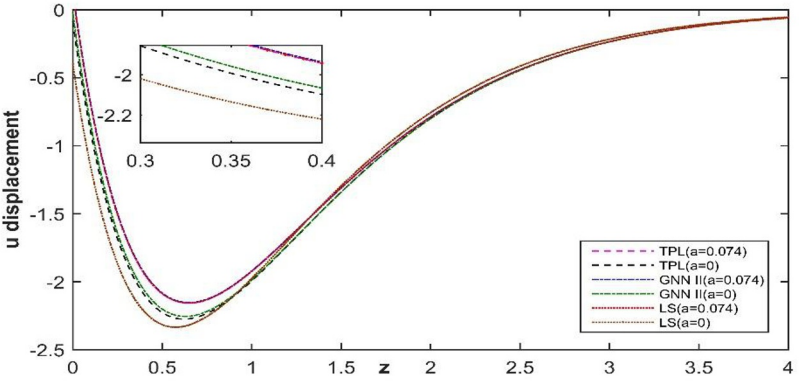

Fig. 2. Two temperature effects on displacement component u

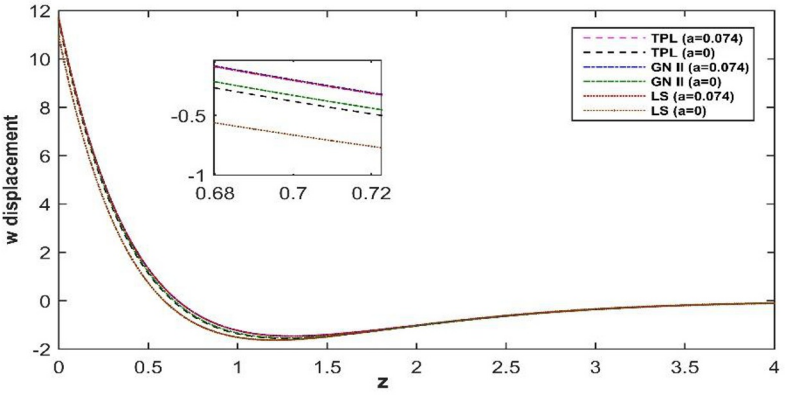

Fig. 3. Two temperature effects on displacement component w

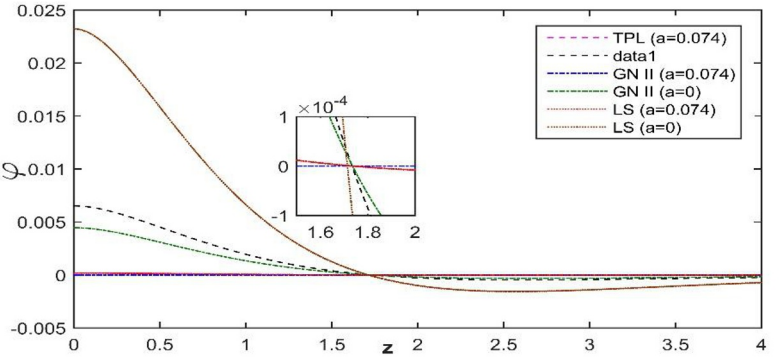

Fig. 4. Two temperature effects on the conductive temperature φ

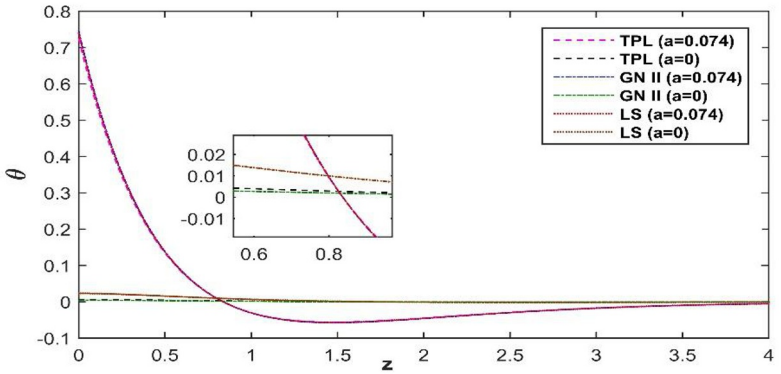

Fig. 5. Two temperature effects on the conductive temperature θ

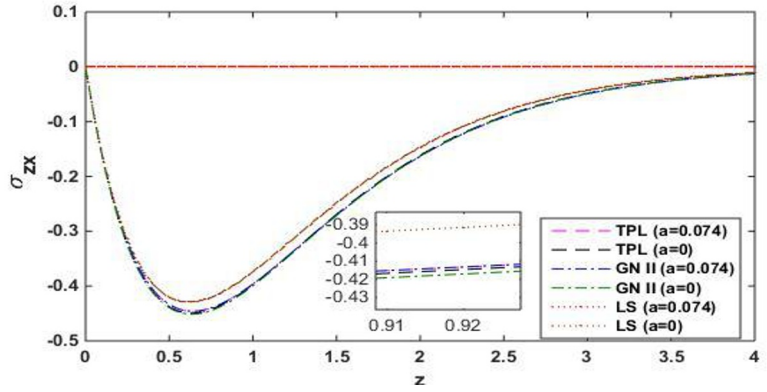

Fig. 6. Two temperature effects on the tangential stress component σ_{zx}

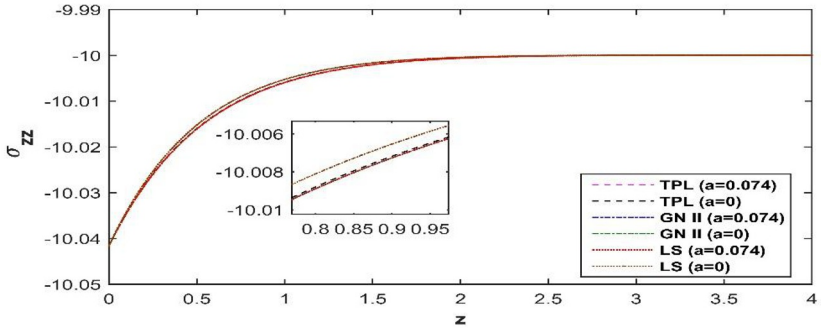

Fig.7. Two temperature effects on the normaal stress component σ_{zz}

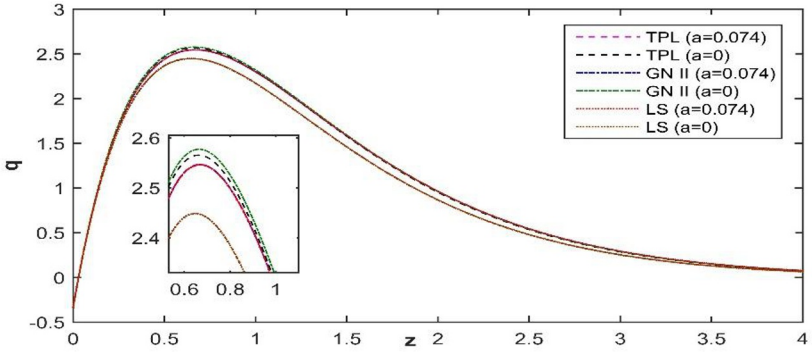

Fig. 8. Two temperature effects on the scalar potential q

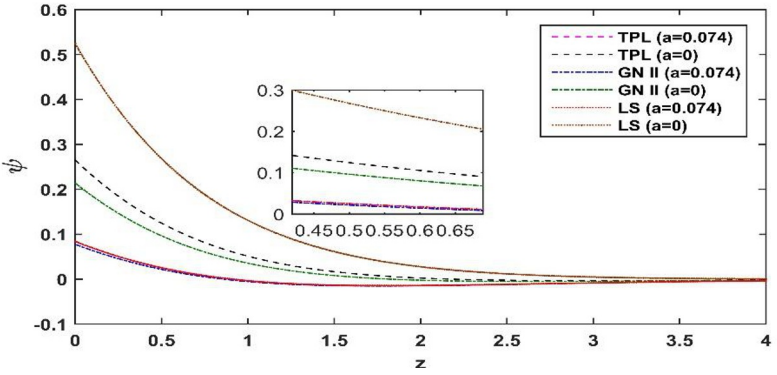

Fig. 9. Two temperature effects on the scalar potential ψ

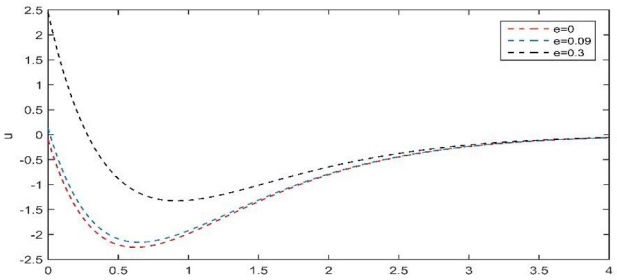

Fig. 10(a). u

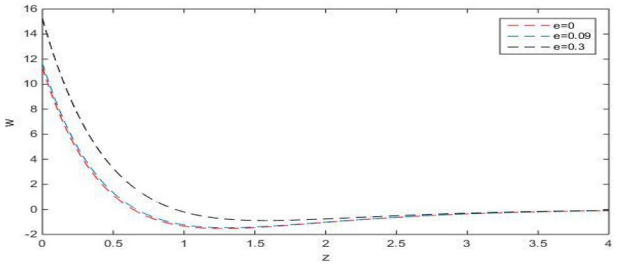

Fig. 10(b). w

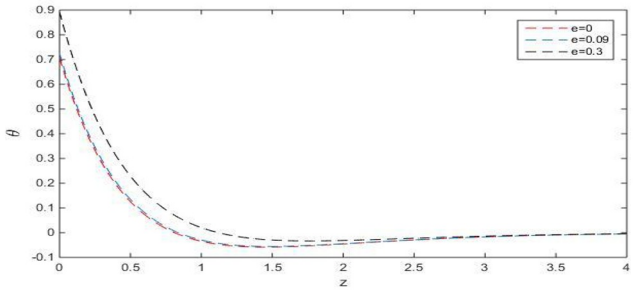

Fig. 10(c). θ

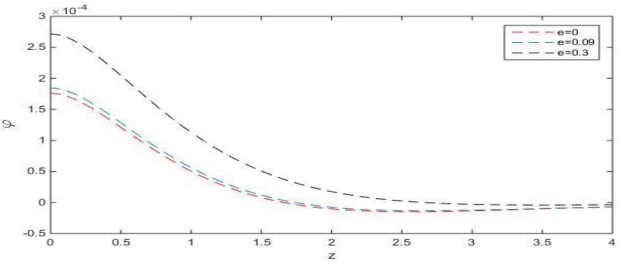

Fig. 10 (d). φ

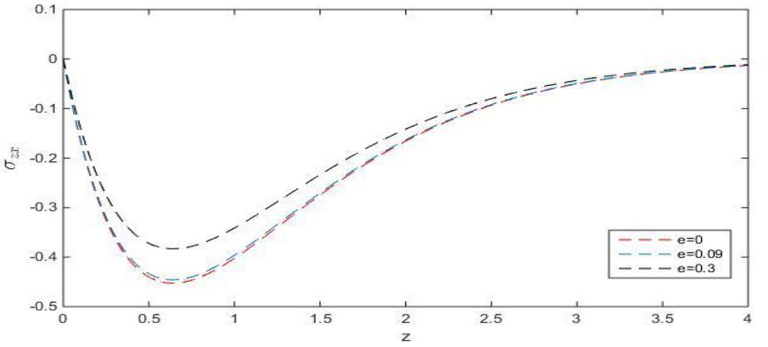

Fig. 10 (e). σ_{zx}

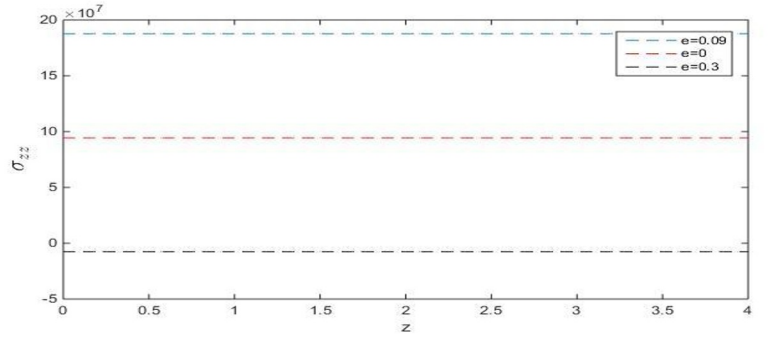

Fig.10 (f). σ_{zz}

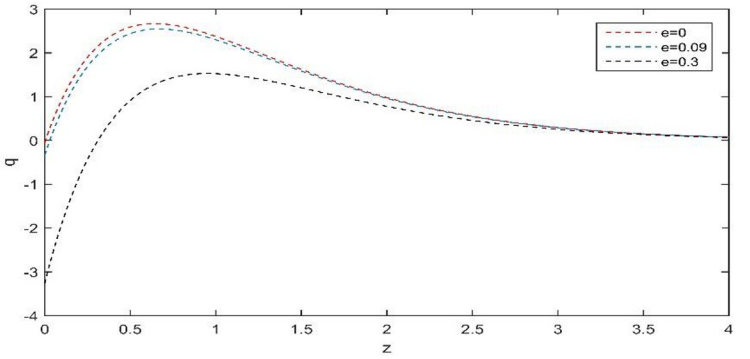

Fig.10(g). q

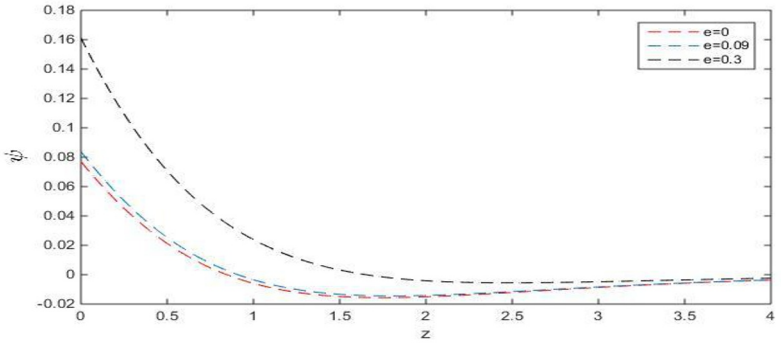

Fig. 10 (h). ψ

Fig. 10. Variation of physical quantities for local & nonlocal theories

Figure 2-9 includes six curves predicted by various thermoelasticity theories. In the figures, dashed lines correspond to the solutions obtained using the three-phase-lag (TPL) model, dashed-dotted lines represent results derived from the generalized thermoelasticity without energy dissipation (G-N II) theory, and dotted lines illustrate solutions based on the Lord-Shulman (L-S) theory. The graphs are shown for two cases, with (a=0.074) and without (a=0) the parameter a, as indicated in the legend.The inset highlights a specific range of z, providing a zoomed-in view of the differences between the theories.

Figure 2 illustrates how different theories of thermoelasticity and two temperature parameter a influence the predicted displacement component u. All curves display a similar behavior: starting with negative displacement values, reaching a minimum and then increasing toward positive values as z progresses.For all theories, the inclusion of a=0.074 shifts the displacement curves slightly compared to when a=0 . The effect of a appears consistent, as it causes minor deviations in the curves, particularly near the minimum displacement.

Figure 3 represents the variation of displacement component w with respect to z for different theoretical models. The displacement w is highest at z = 0 and decreases rapidly as z increases, eventually stabilizing around zero.For each model, the curves with parameter of two temperature (a = 0.074) show a slightly high displacement compared to one temperature (a = 0), indicating that two temperature effects influence displacement.

Figure 4 represents the variation of φ along the spatial coordinate z.Initially φ shows significant variation for all models. For a=0.074, curve of all three theories is close to each other and variation can be seen for a=0. The system stabilizes and φ approaches zero uniformly across all models, regardless of the value of a at larger distances from the origin, and this justifies the real behavior of the system.

Figure 5 shows how the thermodynamic temperature θ varies with respect to z for different thermoelastic models with and without effects of two temperature theory.The temperature θ is highest at z = 0 and decreases rapidly and approaches a near-zero value at higher z, indicating that the thermal effect weakens as the distance

increases.The case (a = 0.074) slightly shifts the temperature values compared to the (a = 0) in all models.

Figure 6 shows the variation of shear stress (σ_{zx}) as a function of z for different thermoelastic models. The stress starts at zero when z = 0 and decreases to a minimum around z = 0.7, reaching its peak negative value.After this point, the stress gradually increases and approaches zero again as z increases beyond 3.5.The Lord-Shulman model (LS) with a = 0 remains nearly constant at zero, indicating minimal stress variation in this case.

Figure 7 depicts the variation of normal stress (σ_{zz}) as a function of z for different thermoelastic models.The stress starts at approximately -10.04 when z = 0 and increases gradually towards -10.00 as z increases. As z grows beyond 2.5, the stress stabilizes, indicating that normal stress becomes nearly constant at larger distances.The stress starts at approximately -10.04 when z = 0 and increases gradually towards -10.00 as z increases.The difference between case (a = 0.074) and the (a = 0) is minimal. The inset zoomed-in section highlights a small gap between these cases, showing that the two temperature parameter slightly influences the stress distribution. The LS model shows a slightly greater deviation compared to TPL and GN II models.Among the models, the Three-Phase Lag (TPL) and Green-Naghdi (GN II) theories behave similarly, while the Lord-Shulman (LS) model shows slightly more deviation.

Figure 8 illustrates behavior of scalar potential q in a thermoelastic medium under different theoretical models in the presesnce and absence of two temperature parameter.The value of q starts from zero at $z = 0$, increases to a peak value around $z = 0.7$, and then gradually decreases towards zero as z increases. The peak value differs slightly between the models for case $a = 0$, as highlighted in the zoomed-in inset. After the peak, all models follow a smooth decline, indicating the dissipation of the scalar potential over distance. Case $(a = 0)$ shows slightly higher peak values than case $(a = 0.074)$ for the TPL and GN II models. The LS model exhibits a relatively lower peak, with $a = 0$ compared to $a = 0.074$. The zoomed-in section emphasizes this difference, particularly for the TPL and GN II models, which display noticeable shifts in peak values.

Figure 9 shows the variation of ψ with respect to z for different thermoelastic models. The curve starts at a positive value for z = 0 and gradually decreases as z increases for all models. This behavior is consistent across all three models, but the magnitude and rate of decay vary. The LS model exhibits the highest initial values of ψ, especially for the nonlocal case (a = 0), as shown by the brown dotted line. The LS model predicts a stronger response, while the TPL and GN II models suggest a more moderate effect. The parameter (a = 0.074) has a visible impact, particularly in the LS model, but as z increases, all models gradually approach a similar behavior.

Figure 10 The three lines are represented with different colors, where black and blue are non- local parameters (e = 0.3, 0.09) respectively and red represents the local parameter (e = 0) and the lines show variations of physical parameters against z. The curves moves initially either in increasing or decreasing manner and at the end they approach to zero, which in turn means the stabilization after a particular distance.

Figure 10(a): The graph describes the variation of horizontal displacement u along with z. The three lines are prominently moving down from their starting points initially slope down with similar gaps with deeper dip and gradually recovers and get combined at the end with stabilization.
Figure 10(b): The graph defines the variation of vertical displacement w with respect to z. The figure clearly reflects that the three curves in the 0<z<1 range decrease slanting down deeply and approaching zero afterward.
Figure 10(c): The graph reports the variation of theta with respect to z. As z increases, all curves show a rapid decline until around z=1.5z, where the rate of decrease slows significantly. Beyond z=2.5, the curves gradually stabilize, converging towards zero by z=4. The influence of e is more pronounced at lower z but diminishes as z increases.
Figure 10(d): The present image reflects the curves starting from a positive value. Black dashed curve (e=0.3) having the highest displacement around 0.17, followed by the blue dashed curve (e = 0.09) and the red dashed curve (e=0) at the lowest. The effect of e is more prominent at lower z, with larger e resulting in higher initial displacement and a slower rate of decay. The curves stabilize and finally tend toward zero.
Figure 10(e): The present figure mentions a variation with a sharp decrease and then reaches the lowest point, after which the curves start to rise gradually and reach zero. The impact of e is more significant in the lower z region, but decreases at higher values of z.
Figure 10(g): The graph shows the variation with respect to Z, the red and blue curves attain a maximum value close to 2.5, while the black curve peaks lower at about 1.5. The curves decreases sharply and reach to lowest point, and the start rising gradually converging towards 0. Higher e results in a lower initial value and peak magnitude.
Figure 10(h): All curves in the figure are initially starting from a negative value and increases with Z. The effect of increasing e results in lower initial values and reduced peak

7. Special Cases

Case I: Neglecting effect of nonlocal and gravity field and two temperature parameters($e = 0, \vartheta = \varphi$ and $g = 0$). the current problem reduces to as obtained by Othman in [41] without diffusion.
Case II: Without gravity($g = 0$) and nonlocal effect ($e = 0$), the system reduces to the same as [23] without rotation.
Case III: Considering thermodynamic temperature equal to conductive temperature ($\vartheta = \varphi$) without magnetic field and initial stress, the medium under study is reduced to research by Said [42] without diffusion.

8. Conclusion

This study highlights several key findings regarding the impact of different factors on the behavior of physical variables in a non-local initial stressed Generalized Magneto thermoelastic medium.
1. The presence of a two temperature parameter significantly influences the physical variables, as demonstrated in Figures (2–9)

2. Influence of Nonlocal Thermoelasticity: The introduction of nonlocal effects alters the behavior of these variables, as evident from Figures (10-16)
3. The problem has been analytically solved using normal mode analysis, a powerful method applicable to various hydrodynamic problems.
4. Physical quantities justify all the considered boundary conditions.The type of boundary conditions and the force exerted influence the way the body deforms.or Body deformation is dependent on the sort of boundary conditions and the force that is applied.
5. The three thermoelastic theories show significant variations in field quantities under the influence of two two-temperature parameter.
6. The three-phase-lag model proves highly useful in applications such as nuclear boiling, exothermic catalytic reactions, phonon-electron interactions, and phonon scattering.

References

1. M. A. Biot, “Thermoelasticity and irreversible thermodynamics,” Journal of applied physics, vol. 27,no. 3, pp. 240–253, 1956.
2. H. W. Lord and Y. Shulman, “A generalized dynamical theory of thermoelasticity,” Journal of the Mechanics and Physics of Solids, vol. 15, no. 5, pp. 299–309, 1967.
3. A. E. Green and K. Lindsay, “Thermoelasticity,” Journal of elasticity, vol. 2, no. 1, pp. 1–7, 1972.
4. I. A. Abbas and A. M. Zenkour, “Ls model on electro–magneto–thermoelastic response of an infinitefunctionally graded cylinder,” Composite Structures, vol. 96, pp. 89–96, 2013.
5. D. Chandrasekharaiah, “Thermoelasticity with second sound: a review,” 1986.
6. D. Y. Tzou, “A unified field approach for heat conduction from macro-to micro-scales,”1995.
7. A. E. Green and P. Naghdi, “A re-examination of the basic postulates of thermomechanics,” Proceedings of the Royal Society of London. Series A: Mathematical and Physical Sciences, vol. 432, no. 1885, pp. 171–194, 1991.
8. A. Green and P. Naghdi, “On undamped heat waves in an elastic solid,” Journal of Thermal stresses,vol. 15, no. 2, pp. 253–264, 1992.
9. A. Green and P. Naghdi, “Thermoelasticity without energy dissipation,” Journal of elasticity, vol. 31,no. 3, pp. 189–208, 1993.
10. I. A. Abbas and A. M. Zenkour, “The effect of magnetic field on thermal shock problem for a fiber-reinforced anisotropic half-space using green-naghdi’s theory,” Journal of Computational and Theoretical Nanoscience, vol. 12, no. 3, pp. 438–442, 2015.
11. R. Quintanilla, “Existence in thermoelasticity without energy dissipation,” Journal of thermal stresses,vol. 25, no. 2, pp. 195–202, 2002.
12. R. S. Dhaliwal and H. H. Sherief, “Generalized thermoelasticity for anisotropic media,” Quarterly of Applied Mathematics, vol. 38, no. 1, pp. 1–8, 1980.
13.] S. R. Choudhuri, “On a thermoelastic three-phase-lag model,” Journal of Thermal Stresses, vol. 30,no. 3, pp. 231–238, 2007.
14. R. Quintanilla and R. Racke, “A note on stability in three-phase-lag heat conduction,” International Journal of Heat and Mass Transfer, vol. 51, no. 1-2, pp. 24–29, 2008.
15. M. Kanoria and S. H. Mallik, “Generalized thermoviscoelastic interaction due to periodically varying heat source with three-phase-lag effect,” European Journal of Mechanics-A/Solids, vol. 29, no. 4, pp. 695–703, 2010.

16. A. S. El-Karamany and M. A. Ezzat, “On the three-phase-lag linear micropolar thermoelasticity theory,”European Journal of Mechanics-A/Solids, vol. 40, pp. 198–208, 2013.
17. M. A. Ezzat, A. S. El Karamany, and M. A. Fayik, “Fractional order theory in thermoelastic solid with three-phase lag heat transfer,” Archive of Applied Mechanics, vol. 82, pp. 557–572, 2012.
18. A. Montanaro et al., “On singular surfaces in isotropic linear thermoelasticity with initial stress,” The Journal of the Acoustical Society of America, vol. 106, pp. 1586–1588, 1999.
19. M. I. Othman and Y. Song, “Reflection of plane waves from an elastic solid half-space under hydrostatic initial stress without energy dissipation,” International Journal of Solids and Structures, vol. 44, no. 17, pp. 5651–5664, 2007.
20. R. Ogden and B. Singh, “Propagation of waves in an incompressible transversely isotropic elastic solid with initial stress: Biot revisited,” Journal of Mechanics of Materials and Structures, vol. 6, no. 1,pp. 453–477, 2011.
21. Z.-H. Qian, F. Jin, T. Lu, K. Kishimoto, and S. Hirose, “Effect of initial stress on love waves in a piezoelectric structure carrying a functionally graded material layer,” Ultrasonics, vol. 50, no. 1, pp. 84–90, 2010.
22. I. A. Abbas and R. Kumar, “2d deformation in initially stressed thermoelastic half-space with voids,”Steel Compos. Struct, vol. 20, no. 5, pp. 1103–1117, 2016.
23. I. Kaur, P. Lata, and K. Singh, “Thermomechanical deformation in a transversely isotropic magneto-thermoelastic rotating solids under initial stress,” Partial Differential Equations in Applied Mathematics,vol. 3, p. 100028, 2021.
24. G. Paria, “Magneto-elasticity and magneto-thermo-elasticity,” Advances in applied mechanics, vol. 10,pp. 73–112, 1966.
25. M. Sadeghi and Y. Kiani, “Generalized magneto-thermoelasticity of a layer based on the lord–shulman and green–lindsay theories,” Journal of Thermal Stresses, vol. 45, no. 4, pp. 319–340, 2022.
26. R. Tiwari, “Analysis of phase lag effect in generalized magneto thermoelasticity with moving heat source,” Waves in Random and Complex Media, vol. 34, no. 3, pp. 1133–1150, 2024.
27. A. K. Yadav, “Reflection of plane waves in a fraction-order generalized magneto-thermoelasticity in arotating triclinic solid half-space,” Mechanics of Advanced Materials and Structures, vol. 29, no. 25, pp. 4273–4290, 2022.
28. A. E. Abouelregal and H. M. Sedighi, “Magneto-thermoelastic behaviour of a finite viscoelastic rotating rod by incorporating eringen’s theory and heat equation including caputo–fabrizio fractional derivative,”Engineering with Computers, vol. 39, no. 1, pp. 655–668, 2023.
29. M. Singh and S. Kumari, “Influence of gravity and initial stress on rayleigh wave propagation in magneto-thermoelastic medium,” J. Math. Comput. Sci., vol. 11, no. 3, pp. 2681–2698, 2021.
30. A. C. Eringen and D. Edelen, “On nonlocal elasticity,” International journal of engineering science,vol. 10, no. 3, pp. 233–248, 1972.
31. A. C. Eringen, “On differential equations of nonlocal elasticity and solutions of screw dislocation and surface waves,” Journal of applied physics, vol. 54, no. 9, pp. 4703–4710, 1983.
32. E. Inan and A. Eringen, “Nonlocal theory of wave propagation in thermoelastic plates,” International journal of engineering science, vol. 29, no. 7, pp. 831–843, 1991.
33. Wang, J., & Dhaliwal, R. S. “Uniqueness in generalized nonlocal thermoelasticity,” Journal of Thermal Stresses, 16(1–2), 71–78, (1993).

34. A. M. Zenkour and A. E. Abouelregal, “Nonlocal thermoelastic vibrations for variable thermal conductivity nanobeams due to harmonically varying heat,” Journal of Vibroengineering, vol. 16, no. 8,pp. 3665–3678, 2014.
35. K. K. Kalkal, S. Deswal, and R. Poonia, “Reflection of plane waves in a rotating nonlocal fiber-reinforced transversely isotropic thermoelastic medium,” Journal of Thermal Stresses, vol. 46, no. 4, pp. 276–292,2023.
36. N. Das, N. Sarkar, and A. Lahiri, “Reflection of plane waves from the stress-free isothermal and insulated boundaries of a nonlocal thermoelastic solid,” Applied Mathematical Modelling, vol. 73, pp. 526–544, 2019.
37. F. S. Bayones, S. Mondal, S. M. Abo-Dahab, and A. A. Kilany, “Effect of moving heat source on a magneto-thermoelastic rod in the context of eringen’s nonlocal theory under three-phase lag with a memory dependent derivative,” Mechanics Based Design of Structures and Machines, vol. 51, no. 5, pp. 2501–2516, 2023.
38. S. Bajaj, A. K. Shrivastav, and S. Kumari, “Effect of Nonlocal Micropolar Thermoelasticity with Initial Stress in the Context of Dual Phase Lag in Thermodynamical Interactions,” *Proceedings of the 2024 International Conference on Control, Computing, Communication and Materials (ICCCCM)*, pp. 494–501, 2024, doi: 10.1109/ICCCCM61016.2024.11039956.M.
39. S. Bajaj, A. K. Shrivastav, and S. Kumari, “Effect of inclined load on plane wave in non-local thermoelastic three-phase lag model,” Palestine Journal of Mathematics, vol.14, no. Special issue 4, pp.53-66, 2025.
40. S. Bajaj and A. K. Shrivastav, “Numerical analysis of thermoelastic wave behavior in a micropolar medium with dual-phase-lag, nonlocality, and pre-stress under gravitational influence,” *Boletim da Sociedade Paranaense de Matemática*, vol. 43, no. 3, pp. 1–25, 2025.
41. I. Othman and E. E. Eraki, “Generalized magneto-thermoelastic half-space with diffusion under initial stress using three-phase-lag model,” Mechanics Based Design of Structures and Machines, vol. 45, no. 2, pp. 145–159, 2017.
42. S. M. Said and M. I. Othman, “2d problem of a nonlocal thermoelastic diffusion solid with gravity via three theories,” Journal of Vibration Engineering & Technologies, vol. 12, no. 4, pp. 5423–5430, 2024.

Open Access This chapter is licensed under the terms of the Creative Commons Attribution-NonCommercial 4.0 International License (http://creativecommons.org/licenses/by-nc/4.0/), which permits any noncommercial use, sharing, adaptation, distribution and reproduction in any medium or format, as long as you give appropriate credit to the original author(s) and the source, provide a link to the Creative Commons license and indicate if changes were made.

The images or other third party material in this chapter are included in the chapter's Creative Commons license, unless indicated otherwise in a credit line to the material. If material is not included in the chapter's Creative Commons license and your intended use is not permitted by statutory regulation or exceeds the permitted use, you will need to obtain permission directly from the copyright holder.